Biochemistry and Biophysics Reports 18 (2019) 100626

Contents lists available at ScienceDirect

Biochemistry and Biophysics Reports

journal homepage: www.elsevier.com/locate/bbrep

Contributions of the C-terminal domain to poly(A)-specific ribonuclease (PARN) stability and self-association

Guang-Jun He, Yong-Bin Yan*

State Key Laboratory of Membrane Biology, School of Life Sciences, Tsinghua University, Beijing, 100084, China

ARTICLE INFO

Keywords:
Deadenylase
Enzyme thermal stability
Enzyme thermal aggregation
Intrinsically disordered domain
Poly(A)-Specific ribonuclease (PARN)
Self-association

ABSTRACT

Poly(A)-specific ribonuclease (PARN) catalyzes the degradation of mRNA poly(A) tail to regulate translation efficiency and mRNA decay in higher eukaryotic cells. The full-length PARN is a multi-domain protein containing the catalytic nuclease domain, the R3H domain, the RRM domain and the C-terminal intrinsically unstructured domain (CTD). The roles of the three well-structured RNA-binding domains have been extensively studied, while little is known about CTD. In this research, the impact of CTD on PARN stability and aggregatory potency was studied by comparing the thermal inactivation and denaturation behaviors of full-length PARN with two N-terminal fragments lacking CTD. Our results showed that K^+ induced additional regular secondary structures and enhanced PARN stability against heat-induced inactivation, unfolding and aggregation. CTD prevented PARN from thermal inactivation but promoted thermal aggregation to initiate at a temperature much lower than that required for inactivation and unfolding. Blue-shift of Trp fluorescence during thermal transitions suggested that heat treatment induced rearrangements of domain organizations. CTD amplified the stabilizing effect of K^+, implying the roles of CTD was mainly achieved by electrostatic interactions. These results suggested that CTD might dynamically interact with the main body of the molecule and release of CTD promoted self-association via electrostatic interactions.

1. Introduction

In eukaryotic cells, gene expression is post-transcriptionally regulated by mRNA 5′- and 3′-untranslational regions. The majority of eukaryotic mRNAs contain a long 3′-end poly(A) tail, which plays a crucial role in mRNA maturation, export from the nucleus, localization, translational efficiency, silencing and decay [1]. The poly(A) tail length is dynamically regulated by the opposing effects of poly(A) polymerases and deadenylases, which elongate or shorten the poly(A) tail length, respectively [2]. Deadenylases, which are 3′-exoribonucleases with a high substrate preference of poly(A) or oligo(A), has been identified to participate in diverse physiological processes such as oocyte maturation, early development, cell cycle, stress response, telomere maintenance and cell migration [3–5]. The importance of deadenylase cellular functions is revealed by the association of inherited mutations or abnormal expression levels of deadenylases with various human diseases [4,6–11].

A number of deadenylases have been identified in eukaryotes [3,4,12]. Among them, poly(A)-specific ribonuclease (PARN, EC 3.1.13.4) has the unique properties of 5′-cap-binding ability, high activity, allosteric regulation, processive catalysis and highly regulated deadenylation in the cells [4,5]. The full-length PARN is a multi-domain enzyme composed of three poly(A) binding domains, the nuclease domain, the R3H domain and the RRM domain (Fig. 1A). Besides these three well-defined domains, PARN also has a C-terminal domain (CTD) predicted to be intrinsically disordered by bioinformatics analysis [13,14]. PARN mainly exists as a homodimer in solutions, while it can also associate into larger oligomers via its R3H domain [15]. The feature of multiple RNA-binding domains is not shared by most deadenylases and may endow PARN to achieve multi-level regulation by the adjustments of domain interactions, interactions with the other proteins or posttranslational modifications. The contributions of the three RNA-binding domains to PARN catalysis, regulation and stability have been well-documented during the past twenty years [4,5]). Biochemical and structural studies have revealed that the nuclease domain of PARN belongs to the DEDD superfamily of 3′-exonucleases with a conserved core structure in this superfamily [16]. Similar to the other members in the DEDD superfamily, PARN utilizes a two-metal-ion catalytic

Abbreviations: CD, circular dichroism; CTD, C-terminal domain; IPTG, isopropyl-1-thio-β-D-galactopyranoside; PARN, poly(A)-specific ribonuclease; p74, the full-length PARN; p60, PARN with the removal of CTD (residues 1–520); p46, PARN with the removal of RRM and CTD (residues 1–446)

* Corresponding author. School of Life Sciences, Tsinghua University, Beijing, 100084, China.
E-mail address: ybyan@tsinghua.edu.cn (Y.-B. Yan).

https://doi.org/10.1016/j.bbrep.2019.100626
Received 26 November 2018; Received in revised form 14 January 2019; Accepted 12 March 2019
Available online 19 March 2019
2405-5808/ © 2019 The Authors. Published by Elsevier B.V. This is an open access article under the CC BY-NC-ND license (http://creativecommons.org/licenses/BY-NC-ND/4.0/).

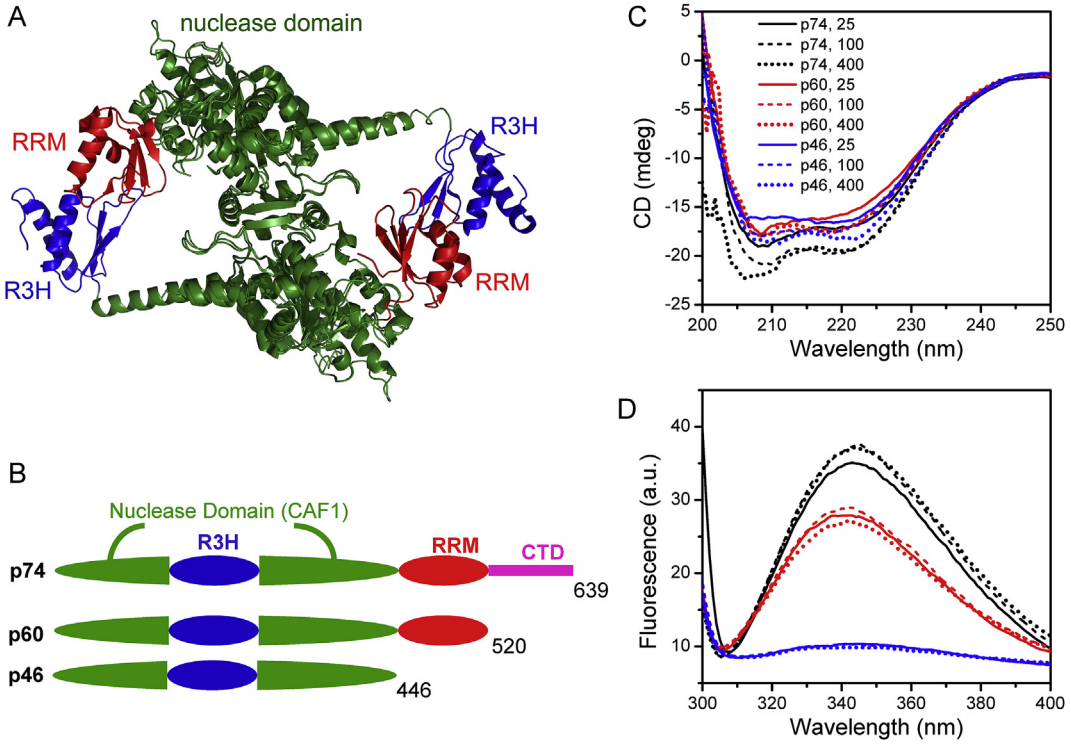

Fig. 1. Domain architecture of PARN and effects of K^+ on p74, p60 and p46 secondary and tertiary structures. (A) Domain organization of the well-folded domains of PARN. The modeled structure was created by aligning the nuclease domain of the crystal structures containing the nuclease and R3H domains (PDB ID: 2A1S) and the nuclease and RRM domains (PDB ID: 3D45). (B) Schematic domain compositions of the full-length PARN and PARN fragments used in this research. (C) Far-UV CD. (D) Intrinsic Trp fluorescence. The spectroscopic experiments were performed by pre-equilibrating proteins in buffer A containing 25 mM, 100 mM or 400 mM K^+. The final protein concentration was 2 μM. The excitation wavelength of the intrinsic fluorescence was 295 nm. All spectroscopic experiments were carried out at 25 °C.

mechanism [16,17]. The most favorable divalent metal ion of PARN is Mg^{2+}, which is not only perquisite for catalysis but also for structural stability [18,19]. The RRM is capable to bind with cap analogue, which may be important for the allosteric regulation and amplified processivity of PARN by the cap structure at the 5′-end of eukaryotic mRNAs [20–23]. However, the role of CTD in PARN functions remains elusive. Previously, two proteolytic fragments with the removal of CTD or removal of CTD and part of the RRM domain has been identified in *Xenopus* and HeLa cell extracts, respectively [24,25], implying that the intracellular functions of PARN may be regulated by proteolysis.

The catalysis of PARN shows a strong dependence on spermidine, K^+ or the other monovalent ions [26,27]. The optimal K^+ concentration is around the physiological concentration in the cells (~100 mM). At least two K^+-binding sites has been proposed to locate at the nuclease domain and RRM domain, which may facilitate PARN catalysis and allosteric regulation, respectively [22]. Similar to most intrinsically disordered regions, CTD of PARN contained a number of positively and negatively charged residues and therefore has the potency to bind with monovalent ions. Low concentrations of chemical denaturants have been proposed to induce CTD structural transition to form more regular secondary structures [14], but it is unclear whether this structural transition can be triggered by physiological factors or not. In this research, we studied the roles of CTD in PARN stability by analyzing the effect of K^+ on the thermal stability of the full-length PARN (p74), the N-terminal fragment lacking CTD (p60) and the fragment lacking CTD and the RRM domain (p46) in the presence of various concentrations of KCl (Fig. 1B). Our results showed that the existence of CTD modulated PARN stability and self-association potency, which could be influenced by the KC concentration. The specific stabilizing effect of K^+ on CTD suggested that electrostatic interactions played a crucial role in adjusting PARN self-association and stability.

2. Materials and methods

2.1. Materials

Tris and kanamycin were purchased from AMRESCO. Imidazole, methylene blue, MOPS and polyadenylic acid potassium salts were obtained from Sigma-Aldrich, Inc. Dithiothreitol (DTT) and isopropyl-1-thio-β-D-galactopyranoside (IPTG) were purchased from Promega. All other reagents were local products of analytical grade.

2.2. Protein expression, purification and sample preparation

The plasmid containing the cDNA sequence of the wild type human PARN was kindly provided by Professor Anders Virtanen (Uppsala University, Sweden). The truncated proteins p60 (residues 1–520 AA) and p46 (residues 1–446 AA) were constructed by standard protocols of mutagenesis using the following primers: p60-forward, 5′-CGATGTCA CATATGGAGATAATCAGGAGC-3'; p60-reverse 5′-GATCCTCGAGCTAC TTCTCTTCCTGTTTTC-3'; p46-forward, 5′-GCTACTCGAGCTTCTCTTCC TGTTTTC-3'; and p46-reverse, 5′-GATCGTCGACTTAATGATCACGTTT AGGCTGC-3'. The obtained genes were cloned to the expression vector pET-28a (Novagen) and verified by sequencing. The recombinant proteins were overexpressed in *Escherichia coli* BL21 (DE3) (Stratagene, Heidelberg, Germany) and purified as described previously [18,28]. In brief, the expression of the proteins was induced by 0.1 mM IPTG at 16 °C for 24 h. The proteins were isolated from the supernatant fraction of cell lysates by Ni^{2+}-affinity chromatography (GE Healthcare),. The final products were purified using a Superdex 200 10/30 GL column equipped on an ÄKTA purifier (GE Healthcare). The protein concentration was determined according to the Bradford method [29]. The protein solutions used for analysis were prepared in buffer A containing 20 mM Tris-HCl (pH 8.0), 100 mM KCl, 0.5 mM DTT, 0.2 mM EDTA and

20% (v/v) glycerol.

2.3. Spectroscopy

Details regarding spectroscopic experiments were the same as those reported previously [30]. In brief, far-UV circular dichroism (CD) spectra were recorded on a Jasco-715 spectrophotometer (Jasco) using a cell with a path length of 0.1 cm. Intrinsic fluorescence spectra were measured on a Hitachi F-2500 spectrophotometer (Hitachi) using a 0.2 mL cuvette with an excitation wavelength of 280 nm or 295 nm. The intrinsic fluorescence of proteins is mainly contributed by Trp and Tyr fluorophores when excited by 280 nm, while dominated by Trp fluorophores when excited at 295 nm. Parameter A, which is a sensitive tool to monitor the position and shape of the Trp fluorescence spectrum [31], was calculated by dividing the fluorescence intensity at 320 nm by that at 365 nm. Resonance Rayleigh light scattering was determined at 90° using an excitation wavelength of 295 nm as described previously [14]. All spectroscopic experiments were carried out using a protein concentration of 2 μM.

2.4. Enzyme assay

The enzymatic activity was measured according to the methylene blue method as described previously [32] with some modifications. In brief, the standard reaction buffer contained 20 mM Tris-HCl, pH 7.0, 100 mM KCl, 1.5 mM $MgCl_2$, 0.5 mM DTT, 0.2 mM EDTA and 10% (v/v) glycerol. Commercial poly(A) was dissolved in the standard reaction buffer with a concentration of 100 μg/ml. The reaction was initiated by mixing 10 μl enzyme and 40 μl substrate solutions and incubated at 37 °C for 8 min. Then methylene blue buffer was added to terminate the reaction and the solution was incubated for another 15 min in the dark. The absorbance at 662 nm was measured using an Ultraspec 4300 pro UV/Visible spectrophotometer. The activity was calculated by a standard curve obtained from the absorbance of commercial poly(A).

2.5. Thermal inactivation

Protein solutions was pre-equilibrated with buffer A containing 25, 100, 400 mM potassium ions at 4 °C. Thermal inactivation was performed by incubating the samples in a water bath for 10 min at a given temperature. Then the samples were cooled on ice and diluted with buffer A containing different concentration of potassium ions to ensure the final concentration of potassium ions were 100 mM in the enzyme assay. The residual activity of each sample was determined using the methylene blue enzyme assay [32]. The presented data were normalized by taking the activity of sample incubated on ice as 1. The standard deviations were calculated from at least three repetitions.

2.6. Thermal denaturation and aggregation

The thermal denaturation of PARN was conducted by incubating the samples containing 2 μM proteins from 30 °C to 85 °C with a temperature interval of 5 °C. The cuvette was sealed by PARAFILM during experiments to avoid changes in solution volumes. At each experimental temperature, the samples were equilibrated for 5 min, and then the intrinsic Trp fluorescence and resonance Rayleigh light scattering were recorded. The aggregation kinetics was measured by measuring the turbidity at 400 nm (A_{400}) with an Ultraspec 4300 pro UV/Visible spectrophotometer using a 1 ml cuvette at 65 °C. The kinetic parameters was analyzed by considering the protein aggregation process as a first-order reaction as described previously [19,33]. The following equation was used for the fitting of the data:

$$A = A_{\lim}(1 - \exp(-k(t - t_0)) \quad (1)$$

where t is the time of incubation at a given temperature, t_0 is the lag time of aggregation, A is turbidity value at time t, $A_{\lim}$ is the A_{400} value at the infinite time and k is the rate constant of the first order reaction. Data fitting was performed by nonlinear regression analysis using Prism (GraphPad Inc.).

3. Results

K^+ is essential to PARN activity [26,27] and acts as an allosteric activator of PARN with multiple binding sites [22]. The potential interactions between K^+ and CTD could not deciphered from activity studies due to the little impact of CTD on PARN catalysis [22]. To address this problem, spectroscopic experiments were carried out for proteins with or without CTD (Fig. 1B) in the presence of 25, 100 and 400 mM K^+. Far-UV CD spectra (Fig. 1C) indicated that high concentrations of K^+ concentrations led to an increase in the ellipticities without significant changes in the shape of the CD spectra, suggesting that the binding of K^+ could induce more regular secondary structures for all of the three proteins. The effect of K^+ on PARN secondary structures was more pronounced for the full-length protein p74 than the two N-terminal fragments lacing CTD. Intrinsic fluorescence excited at 295 nm, which reflects the microenvironments of Trp fluorophores, was used to probe the tertiary structural changes (Fig. 1D). Although the fluorescence intensity of the three proteins differed significantly due to the dissimilar numbers of Trp fluorophores, the position and the shape of the intrinsic fluorescence spectra was not altered by the increase of K^+ concentrations.

Protein stability can evaluate how protein structures are modified by the binding of co-solutes. In the Hofmeister series, K^+ has long been characterized as a chaotrope with minor protein destabilization ability [34]. To examine whether K^+ influenced PARN via the general Hofmeister effect, the thermally induced inactivation, denaturation and aggregation was monitored for the three proteins in the presence of 25, 100 and 400 mM K^+ (Fig. 2). To facilitate the comparison of the results, all transition curves were fitted by a two-state model. The results showed that K^+ could successful protect all of the three proteins against thermal inactivation and denaturation. Among the three enzymes, the full-length enzyme p74 was the most stable against thermal inactivation under all K^+ concentrations (Fig. 2B). When K^+ concentration was increased from 25 mM to 400 mM, the $\Delta T_{0.5}$-inactivation, which is the changes of the midpoint temperature of thermal inactivation, was 9.4 °C, 4.8 °C and 4.0 °C for p74, p60 and p46, respectively. Thus the existence of CTD could successfully protect PARN against unfolding of the active site structure and the protective effect of K^+ on enzyme activity was much more significant when PARN possessed CTD.

The effects of K^+ on the increase of the overall structural stability was similar for the three proteins as evaluated by the midpoint temperature of denaturation monitored by intrinsic fluorescence (Fig. 2D). It is worth noting that during protein unfolding, the Trp fluorescence usually red-shifted with a decrease in the Parameter A value due to the exposure of interior Trp fluorophores to solvent. For example, Trp fluorophores in PARN red-shifted to a value similar to free Trp when fully denatured by chemical denaturants [14,28]. Unexpectedly, the Trp fluorescence of all three proteins had a blue-shift and therefore an increase of Parameter A (Fig. 2C). The blue-shift of Trp fluorescence indicated that the Trp fluorophores were in more hydrophobic microenvironments rather than exposed to the solvent during PARN thermal denaturation. This unusual behavior might be caused by either a more compact structure at high temperatures or the formation of high-order oligomers, which protected some of the Trp fluorophores from solvent-exposure. The similar patterns of the three proteins suggested that this unusual blue-shift was not caused by the RRM domain or CTD. There is only one Trp residue in p46, W219 at the R3H domain (Fig. 3A). Thus this unusual behavior of Trp fluorescence is likely to be caused by conformational changes of the R3H domain.

R3H domain-trigged self-association has been shown to led to blue-shift of Trp fluorescence in p46 [15]. However, no large oligomers or protein aggregates could be detected below 50 °C for p46 (Fig. 2E). To

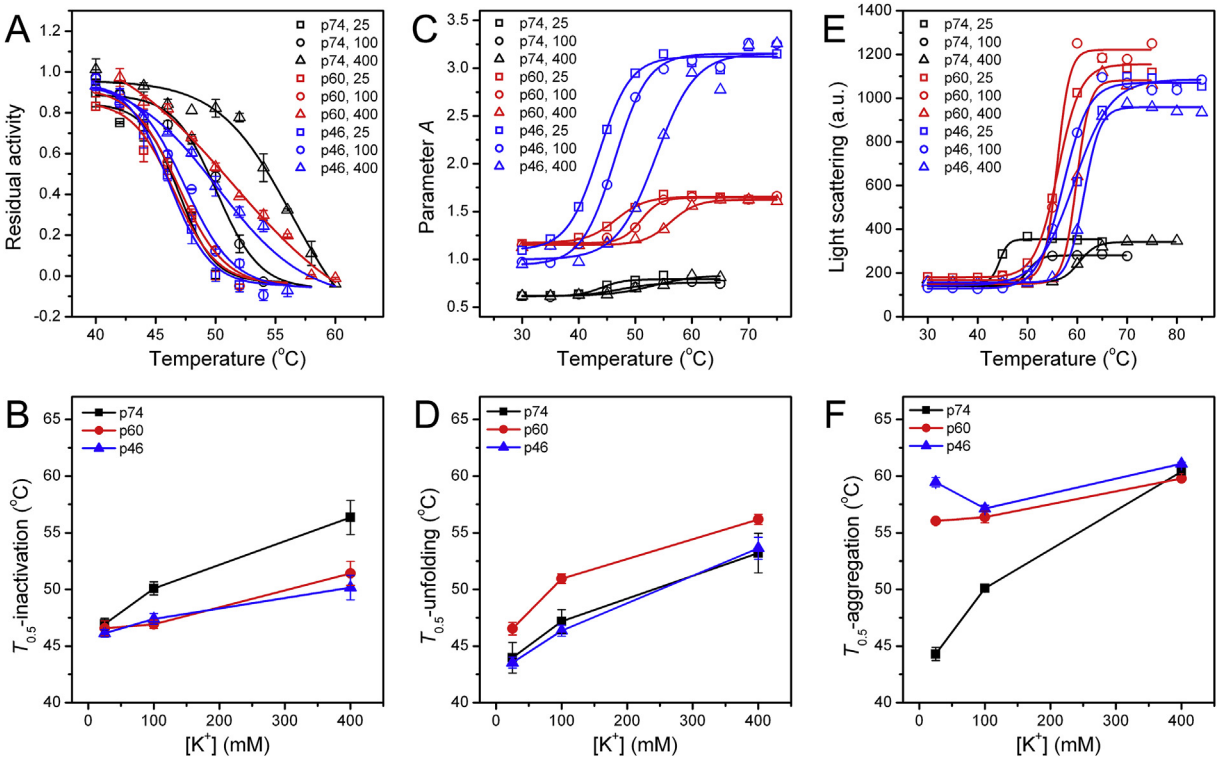

Fig. 2. Effect of K^+ on the thermal stability of p74 (black), p60 (red) and p46 (blue). (A) Thermal inactivation transition curves. Enzymes were pre-equilibrated with buffer A containing 25 mM (squares), 100 mM (circles) or 400 mM (triangles) K^+ at 4 °C. After heat treatment, the samples were cooled on ice and diluted in buffer A containing different concentration of K^+ to ensure a final concentration of 100 mM K^+ in the activity assay. The residual activity was normalized by taking the activity of sample incubated on ice as 1. The mean value and the standard deviations were calculated from at three repetitions. (B) Concentration-dependent effect of K^+ on the midpoint temperature of thermal inactivation ($T_{0.5}$-inactivation). (C) Thermal denaturation transition curves monitored by Parameter *A* of Trp fluorescence. Parameter *A* is the ratio of the intensity of the intrinsic fluorescence at 320 nm to that at 365 nm (I_{320}/I_{365}). (D) Concentration-dependent effect of K^+ on the midpoint temperature of thermal unfolding ($T_{0.5}$-unfolding). (E) Thermal aggregation transition curves monitored by light scattering. Light scattering was recorded at 90° with an excitation wavelength of 295 nm. (F) Concentration-dependent effect of K^+ on the midpoint temperature of thermal aggregation ($T_{0.5}$-aggregation).

further elucidate whether the heat-induced blue-shift of Trp fluorescence was caused by conformational changes or oligomerization, the intrinsic fluorescence of Tyr and Trp fluorophores of p46 was measured simultaneously using an excitation wavelength of 280 nm or 295 nm. Tyr fluorescence is centered at 305 nm (Fig. 3B), while Trp fluorescence is at around 330 nm as determined by the Trp fluorescence spectra with an excitation wavelength of 295 nm (Fig. 3D). If heat treatment only promotes non-specific fluorescence quenching but not conformational change, the intensities of Tyr and Trp fluorescence are expected to decrease simultaneously without significant alternations in the spectral shape. If change in intrinsic fluorescence is induced by protein oligomerization/aggregation, synchronous change is expected for the intensities of Tyr and Trp fluorescence. The results in Fig. 3C and E clearly indicated that the fluorescence quantum yields changed asynchronously for the Tyr and Trp fluorophores when temperature increased. The Tyr fluorescence decreased linearly as a function of temperature (Fig. 3C), coincided with the fact that higher temperature can accelerate fluorescence quenching by promoting Brownian motions of proteins and solvent molecules. On the contrary, the Trp fluorescence increased at low temperatures and followed by a linear decrease at high temperatures (Fig. 3C and E). The linear decrease of the widely distributed Tyr fluorophores (Fig. 3A) indicated that the overall structure changed little upon heating. The unusual increase of the Trp fluorescence quantum yield suggested that the R3H domain might have a rigid-body movement, which led to a more compact quaternary structure as temperature increased from 35 °C to 55 °C. This hypothesis is likely to be true since the R3H domain is extruded from the nuclease domain in the crystal structure of p46 (Fig. 3A) and no significantly changes in secondary structures when monitored by far-UV CD (data not shown).

The formation of non-native aggregates was monitored by resonance Rayleigh light scattering, which is a sensitive tool to monitor the appearance of large oligomers/aggregates in solutions [14]. The K^+ concentration-dependence of the three proteins behaved quite differently. An opposing action of K^+ was observed between p74 and p46 at low K^+ concentrations (Fig. 2E and F). K^+ could efficiently protect p74 against aggregation with an increase of the $T_{0.5}$-aggregation value of 16 °C when K^+ concentration was increased from 25 mM to 400 mM, while p60 was weakly protected by K^+ with $\Delta T_{0.5}$-aggregation = 3.7 °C. The aggregation of p46 in the presence of 100 mM K^+ was the most serious, and 400 mM K^+ could slightly retard the appearance of aggregates. It is worth noting that p74 was the most aggregation-prone in buffers with low K^+ concentrations, while the $T_{0.5}$-aggregation values were almost identical for the three proteins in the presence of 400 mM K^+. These observations suggested that the existence of CTD facilitated PARN aggregation and the dramatic protection of K^+ on p74 thermal aggregation was achieved via specific binding with CTD.

Aggregation kinetics at 65 °C was studied to quantitatively evaluate the effects of K^+ on the aggregation behavior of PARN (Fig. 4). Consistent with the equilibrium thermal denaturation studies, p74 was the most aggregation-prone, followed by p60, while p46 was the least. With the addition of K^+, the aggregation of p74 was significantly inhibited to a level close to that of p60. On the contrary, K^+ promoted the aggregation of p60 and p46, and saturated when K^+ concentration reached 100 mM. The aggregation kinetic parameters were obtained by

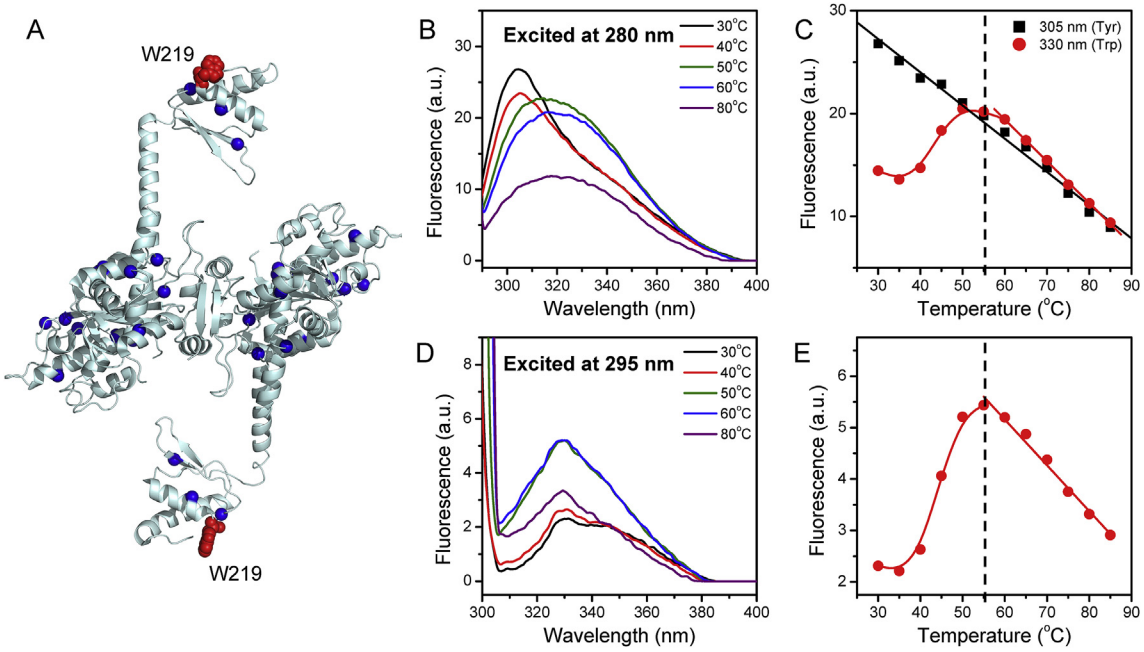

Fig. 3. Thermal transition of p46 monitored by intrinsic fluorescence excited at 280 nm or 295 nm. (A) Positions of Trp and Tyr fluorophores in dimeric p46 created from the crystal structure of PARN (PDB ID: 2A1S). The Trp fluorophores are highlighted by the sphere model in red, while C_α of Tyr residues are highlighted by the ball model in blue. (B) Tyr and Trp fluorescence changes of p46 as a function of temperature determined by excited at 280 nm. (C) Temperature dependence of the fluorescence intensities at 305 nm and 330 nm, representing fluorescence arisen from Tyr and Trp fluorophores when excited at 280 nm, respectively. (D) Trp fluorescence spectra of p46 at various temperatures determined by excited at 295 nm. (E) Temperature dependence of the Trp fluorescence intensities at 330 nm. The experiments were performed using p46 in buffer with 25 mM KCl, while similar results were also observed for p46 in buffer with the addition of 100 or 400 mM KCl (data not shown).

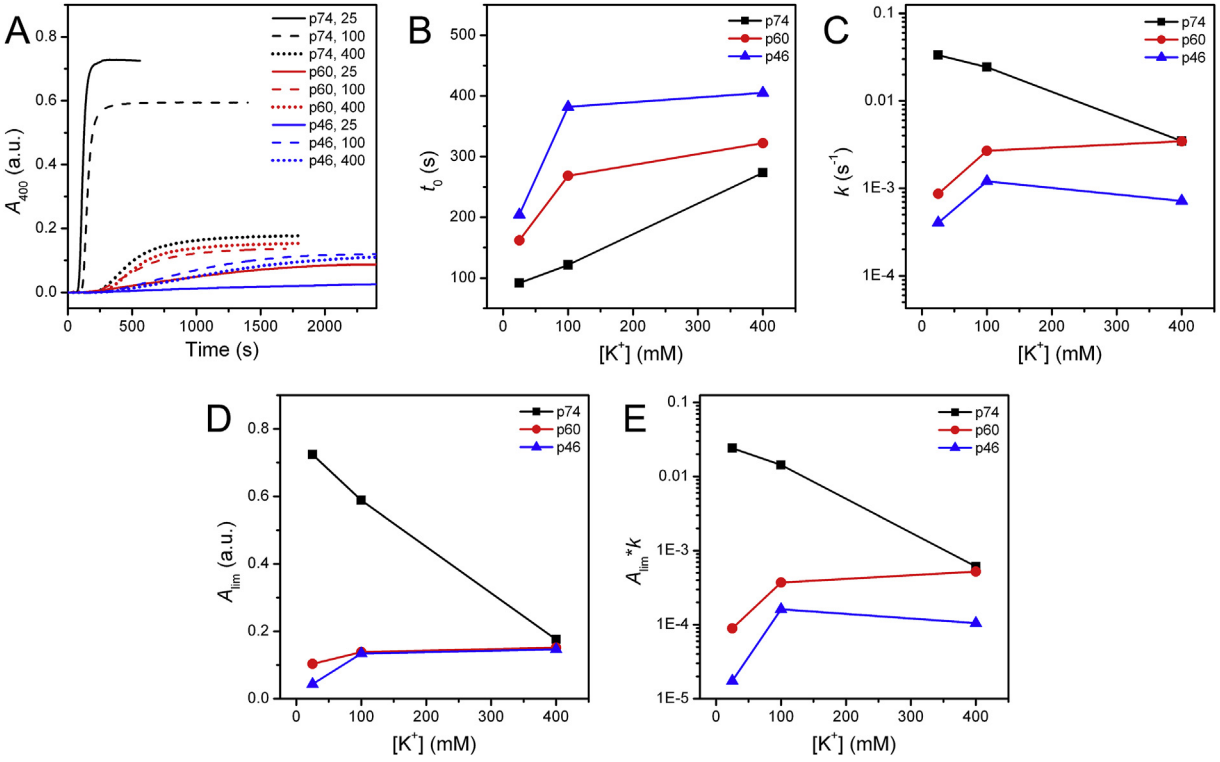

Fig. 4. Effect of K^+ on the aggregation kinetics of p74 (black), p60 (red) and p46 (blue). (A) Raw data of the time-course aggregation of the proteins. Enzymes were pre-equilibrated with buffer A containing various concentrations of K^+ at 4 °C. The aggregation of the samples was monitored by measuring the turbidity at 400 nm (A_{400}) at 65 °C controlled by a water-bath. The final concentration of the protein was 2 μM. Concentration-dependent effects of K^+ on the kinetic parameters of aggregation are shown in panels B–E. (B) Lag time of aggregation (t_0). (C) Aggregation rate constant (k). (D) A_{400} value at the infinite time (A_{lim}). (E) Initial velocity of thermal aggregation obtained by k^*A_{lim}.

fitting of the time-course changes in turbidity by Eq. (1). Increase of K^+ concentration could elongate the lag time (t_0) of aggregation for all of the three proteins. Notably, aggregation occurred at a higher temperature than unfolding during equilibrium thermal denaturation (Fig. 2). The elongation of t_0 by K^+ was resulted from the stabilization of the proteins against thermal unfolding. Thus the thermal aggregation of all three proteins followed an unfolding-limited aggregation model, in which the conformational change is the rate-limiting step for the onset of aggregation. K^+ could inhibit p74 aggregation by decreasing both k and A_{lim}, but promote p60 and p46 aggregation by increasing k and A_{lim}. The aggregation-promoting effect of K^+ on p60 and p46 might be caused by the general effect of salt on protein aggregation [35]. The opposing effects of K^+ on the aggregation behaviors between PARN with or without CTD could be clearly observed from the changes of k^*A_{lim} (Fig. 4E), which reflects the initial velocity of aggregation and is an excellent indicator to examine the actions of various factors [33]. The distinct K^+-concentration dependence of the three proteins revealed that CTD was an aggregation-prone domain and K^+ could modulate the aggregatory potency of PARN via binding with CTD.

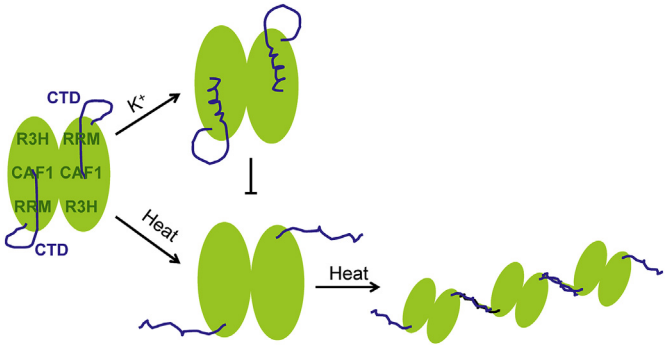

Fig. 5. A proposed model of the role of CTD in PARN stability and self-association. At low K^+ concentrations, CTD binds with the core of the protein containing three RNA-binding domains weakly. The interaction between CTD and protein core structure can be disrupted by mild heat treatment and the released CTD triggers self-association. High concentrations of K^+ induce additional regular secondary structures in CTD to bind with protein core structure more tightly and thereby stabilize PARN by inhibiting the release of CTD during heat treatment.

4. Discussion

The structural and functional roles of the three RNA-binding domains of PARN have been extensively explored by structural, biophysical and biochemical studies (reviewed in Ref. [5]). However, little is known about CTD of PARN, which contains about 120 amino acid residues and is predicted to be intrinsically unstructured [13,14]. The existence of two PARN proteolytic fragments with the removal of CTD in *Xenopus* and HeLa cell extracts [24,25] implies that CTD may have regulatory roles in the cells. Due to its intrinsically unstructured nature, CTD contributes little to PARN catalysis [22,30]. In this research, we investigated the impact of CTD on PARN stability and response to salts by comparing the thermal properties of proteins with or without CTD in the presence of difference concentrations of K^+. Our results showed that CTD could modulate PARN stability and aggregatory potency. The actions of CTD could be modulated by K^+ concentrations. Our findings provide insights in understanding the structural role of CTD and regulation of PARN function by electrostatic interactions.

The existence of CTD may be important to the structural integrity of PARN. Notably, under all K^+ concentration conditions, the stability of p74 against thermal inactivation was the highest among the three enzymes regardless of its aggregation-prone property (Fig. 2). Particularly at high K^+ concentrations, p74 had similar aggregation behavior to p60 and p46, but a pronounced high stability against inactivation induced by heat. The structural basis of this unusual property of PARN possessing CTD remains unknown. A possible explanation is that CTD weakly binds with the RNA-binding domains via electrostatic interactions and the binding is reinforced by high K^+ concentrations. At high K^+ concentrations, the tighter binding of CTD with the other domains might result from high K^+ concentration-induced more regular secondary structures (Fig. 1C) with higher binding ability. Based on the results obtained herein, a hypothetical model is shown in Fig. 5. This hypothesis is consistent with the previously AFM result, which showed that the full-length PARN has a compact globular architecture [13]. The interaction interface between CTD and the RNA-binding domains did not interfere with the binding sites of substrate and allosteric regulators [22] but enhanced domain stability against heat-induced inactivation (Fig. 2). Furthermore, the interaction between CTD and the RNA-binding domains was probably highly dynamic with a large dissociation constant and involves only part of CTD. That's why this interaction is difficult to be probed by high-resolution structural studies or spectroscopic methods, but can only get hints from stability analysis.

A comparison of the thermal transition curves of the three proteins suggested that the existence of CTD affected the thermal denaturation mechanism of PARN. For the two proteins lacking either CTD or CTD and RRM, the thermal aggregation occurred at a temperature much higher than inactivation and structural changes under all K^+ concentration conditions, suggesting that the onset of aggregation required total inactivation of the enzymes accompanied with significant conformational changes of the molecules. As for p74, aggregation occurred at a temperature where the enzyme had no significant changes in its activity and structure at low K^+ concentrations. In the presence of 25 mM and 100 mM K^+, the $T_{0.5}$ values for inactivation of p74 were higher than those for unfolding and aggregation. This suggested that the full-length protein possessing CTD could maintain its catalytic activity and native-like structure at the early stage of aggregation. During thermal denaturation, the secondary structures changed little as revealed by the almost superimposed CD spectra before serious aggregation occurred (data not shown, see also [18]). Although there was an alteration in the Trp fluorescence during thermal denaturation, the unusual blue-shift of Trp fluorescence was not arose from the complete deanturation of the molecule but from structural adjustment of the domain organization. The discrepancy of the thermal denaturation behavior of the three proteins indicated that CTD was an aggregation-prone domain that mediated PARN assembled into aggregates with native-like structures under mild denaturing conditions (Fig. 5). Actually, it has been shown that some enzymes can form amyloid-like fibrils with native-like structures and activity [36]. The aggregatory potency of the full-length PARN was significantly weakened by 400 mM K^+, suggesting that electrostatic interactions was the main driving force for the aggregation of p74. Previously PARN has been shown to be able to self-associate into active tetramers or high-order oligomers triggered by hydrophobic interactions of the R3H domain under physiological KCl concentrations [15]. The results herein further suggested that self-association of PARN could also triggered by CTD via electrostatic interactions. The dynamic self-association facilitated the cells to concentrate PARN molecules in desired micro-domains or compartments and to achieve highly regulated deadenylation. Further research is needed to explore the physiological implications of PARN self-association trigged by CTD and the R3H domain.

It is worth noting that the other deadenylases, CCR4-Caf1 and Pan2-Pan3, have been shown to be able to localize in large cytoplasmic RNA granules [37,38]. Domain with low complexity has been proposed to be crucial to the assembly of the RNA granule components including CCR4 and Caf1 [39–42]. It is unclear yet whether the intrinsically unstructured CTD is involved in the recruitment of PARN to large protein complexes such as CPEB-containing complex [43] or exosome-containing RNA granules [44]. Our findings that CTD is an aggregation-prone domain at physiological K^+ concentrations suggested that CTD might play a role in mediating PARN recruitment into the above protein

complexes or granules with the maintenance of its native-like structures and catalytic activity. Meanwhile, intrinsically unstructured domains has been proposed to be capable to interact with multiple targets accompanied with a structural transition to a folded form [45], which supported the idea that both PARN self-association and protein-protein interactions could be triggered by the intrinsically unstructured CTD. Thus in the cells, the proteolysis of PARN might modify PARN functions by altering its self-association ability as well as protein interacting network.

Author contributions

Conceived and designed the experiments: Y.-B. Y. Performed the experiments: G.-J. H. Analyzed the data: G.-J. H. and Y.-B. Y. Wrote the paper: Y.-B. Y.

Declaration of competing interests

None.

Acknowledgements

This study was supported by the National Natural Science Foundation of China [grant numbers 31870783, 31370797]. The authors thank Dr. W. Liu for suggestions.

Transparency document

Transparency document related to this article can be found online at https://doi.org/10.1016/j.bbrep.2019.100626

References

[1] N.L. Garneau, J. Wilusz, C.J. Wilusz, The highways and byways of mRNA decay, Nat. Rev. Mol. Cell Biol. 8 (2007) 113–126.
[2] J.H. Kim, J.D. Richter, Opposing polymerase-deadenylase activities regulate cytoplasmic polyadenylation, Mol. Cell 24 (2006) 173–183.
[3] A.C. Goldstrohm, M. Wickens, Multifunctional deadenylase complexes diversify mRNA control, Nat. Rev. Mol. Cell Biol. 9 (2008) 337–344.
[4] Y.B. Yan, Deadenylation: enzymes, regulation, and functional implications, Wiley Interdiscip. Rev. RNA 5 (2014) 421–443.
[5] A. Virtanen, N. Henriksson, P. Nilsson, M. Nissbeck, Poly(A)-specific ribonuclease (PARN): an allosterically regulated, processive and mRNA cap-interacting deadenylase, Crit. Rev. Biochem. Mol. Biol. 48 (2013) 192–209.
[6] L.-N. Zhang, Y.-B. Yan, Depletion of poly(A)-specific ribonuclease (PARN) inhibits proliferation of human gastric cancer cells by blocking cell cycle progression, Biochim. Biophys. Acta Mol. Cell Res. 1853 (2015) 522–534.
[7] P. Maragozidis, E. Papanastasi, D. Scutelnic, A. Totomi, I. Kokkori, S.G. Zarogiannis, T. Kerenidi, K.I. Gourgoulianis, N.A. Balatsos, Poly(A)-specific ribonuclease and Nocturnin in squamous cell lung cancer: prognostic value and impact on gene expression, Mol. Canc. 14 (2015) 187.
[8] P. Maragozidis, M. Karangeli, M. Labrou, G. Dimoulou, K. Papaspyrou, E. Salataj, S. Pournaras, P. Matsouka, K.I. Gourgoulianis, N.A. Balatsos, Alterations of deadenylase expression in acute leukemias: evidence for poly(a)-specific ribonuclease as a potential biomarker, Acta Haematol. 128 (2012) 39–46.
[9] N.A. Balatsos, P. Maragozidis, D. Anastasakis, C. Stathopoulos, Modulation of poly (A)-specific ribonuclease (PARN): current knowledge and perspectives, Curr. Med. Chem. 19 (2012) 4838–4849.
[10] H. Tummala, A. Walne, L. Collopy, S. Cardoso, J. de la Fuente, S. Lawson, J. Powell, N. Cooper, A. Foster, S. Mohammed, V. Plagnol, T. Vulliamy, I. Dokal, Poly(A)-specific ribonuclease deficiency impacts telomere biology and causes dyskeratosis congenita, J. Clin. Investig. 125 (2015) 2151–2160.
[11] D.H. Moon, M. Segal, B. Boyraz, E. Guinan, I. Hofmann, P. Cahan, A.K. Tai, S. Agarwal, Poly(A)-specific ribonuclease (PARN) mediates 3'-end maturation of the telomerase RNA component, Nat. Genet. 47 (2015) 1482–1488.
[12] N. Izumi, K. Shoji, Y. Sakaguchi, S. Honda, Y. Kirino, T. Suzuki, S. Katsuma, Y. Tomari, Identification and functional analysis of the pre-piRNA 3' trimmer in silkworms, Cell 164 (2016) 962–973.
[13] A. Niedzwiecka, M. Lekka, P. Nilsson, A. Virtanen, Global architecture of human poly(A)-specific ribonuclease by atomic force microscopy in liquid and dynamic light scattering, Biophys. Chem. 158 (2011) 141–149.
[14] G.J. He, A. Zhang, W.F. Liu, Y. Cheng, Y.B. Yan, Conformational stability and multistate unfolding of poly(A)-specific ribonuclease, FEBS J. 276 (2009) 2849–2860.
[15] G.J. He, Y.B. Yan, Self-association of poly(A)-specific ribonuclease (PARN) triggered by the R3H domain, Biochim. Biophys. Acta 1844 (2014) 2077–2085.
[16] M.S. Wu, M. Reuter, H. Lilie, Y.Y. Liu, E. Wahle, H.W. Song, Structural insight into poly(A) binding and catalytic mechanism of human PARN, EMBO J. 24 (2005) 4082–4093.
[17] Y.-G. Ren, L.A. Kirsebom, A. Virtanen, Coordination of divalent metal ions in the active site of poly(A)-specific ribonuclease, J. Biol. Chem. 279 (2004) 48702–48706.
[18] W.F. Liu, A. Zhang, Y. Cheng, H.M. Zhou, Y.B. Yan, Effect of magnesium ions on the thermal stability of human poly(A)-specific ribonuclease, FEBS Lett. 581 (2007) 1047–1052.
[19] G.J. He, W.F. Liu, Y.B. Yan, Dissimilar roles of the four conserved acidic residues in the thermal stability of poly(A)-specific ribonuclease, Int. J. Mol. Sci. 12 (2011) 2901–2916.
[20] P. Nilsson, N. Henriksson, A. Niedzwiecka, N.A.A. Balatsos, K. Kokkoris, J. Eriksson, A. Virtanen, A multifunctional RNA recognition motif in poly(A)-specific ribonuclease with cap and poly(A) binding properties, J. Biol. Chem. 282 (2007) 32902–32911.
[21] T. Monecke, S. Schell, A. Dickmanns, R. Ficner, Crystal structure of the RRM domain of poly(A)-specific ribonuclease reveals a novel m^7G-cap-binding mode, J. Mol. Biol. 382 (2008) 827–834.
[22] W.F. Liu, A. Zhang, Y. Cheng, H.M. Zhou, Y.B. Yan, Allosteric regulation of human poly(A)-specific ribonuclease by cap and potassium ions, Biochem. Biophys. Res. Commun. 379 (2009) 341–345.
[23] M. Wu, P. Nilsson, N. Henriksson, A. Niedzwiecka, M.K. Lim, Z. Cheng, K. Kokkoris, A. Virtanen, H. Song, Structural basis of m^7GpppG binding to poly(A)-specific ribonuclease, Structure 17 (2009) 276–286.
[24] C.G. Körner, M. Wormington, M. Muckenthaler, S. Schneider, E. Dehlin, E. Wahle, The deadenylating nuclease (DAN) is involved in poly(A) tail removal during the meiotic maturation of *Xenopus* oocytes, EMBO J. 17 (1998) 5427–5437.
[25] J. Martìnez, Y.G. Ren, A.C. Thuresson, U. Hellma, J. Åström, A. Virtanen, A 54-kDa fragment of the poly(A)-specific ribonuclease is an oligomeric, processive, and cap-interacting poly(A)-specific 3' exonuclease, J. Biol. Chem. 275 (2000) 24222–24230.
[26] C.G. Körner, E. Wahle, Poly(A) tail shortening by a mammalian poly(A)-specific 3'-exoribonulease, J. Biol. Chem. 272 (1997) 10448–10456.
[27] J. Åström, A. Åström, A. Virtanen, Properties of a HeLa cell 3' exonuclease specific for degrading poly(A) tails of mammalian mRNA, J. Biol. Chem. 267 (1992) 18154–18159.
[28] A. Zhang, W.F. Liu, Y.B. Yan, Role of the RRM domain in the activity, structure and stability of poly(A)-specific ribonuclease, Arch. Biochem. Biophys. 461 (2007) 255–262.
[29] M.M. Bradford, A rapid and sensitive method for the quantitation of microgram quantities of protein utilizing the principle of protein-dye binding, Anal. Biochem. 72 (1976) 248–252.
[30] G.J. He, A. Zhang, W.F. Liu, Y.B. Yan, Distinct roles of the R3H and RRM domains in poly(A)-specific ribonuclease structural integrity and catalysis, Biochim. Biophys. Acta 1834 (2013) 1089–1098.
[31] K.K. Turoverov, S.Y. Haitlina, G.P. Pinaev, Ultra-violet fluorescence of actin. Determination of native actin content in actin preparations, FEBS Lett. 62 (1976) 4–6.
[32] Y.A. Cheng, W.F. Liu, Y.B. Yan, H.M. Zhou, A nonradioactive assay for poly(A)-specific ribonuclease activity by methylene blue colorimetry, Protein Peptide. Lett. 13 (2006) 125–128.
[33] B.I. Kurganov, Kinetics of protein aggregation. Quantitative estimation of the chaperone-like activity in test-systems based on suppression of protein aggregation, Biochemistry (Mosc.) 67 (2002) 409–422.
[34] P. Lo Nostro, B.W. Ninham, Hofmeister phenomena: an update on ion specificity in biology, Chem. Rev. 112 (2012) 2286–2322.
[35] Y.B. Yan, J. Zhang, H.W. He, H.M. Zhou, Oligomerization and aggregation of bovine pancreatic ribonuclease A: characteristic events observed by FTIR spectroscopy, Biophys. J. 90 (2006) 2525–2533.
[36] F. Chiti, C.M. Dobson, Amyloid formation by globular proteins under native conditions, Nat. Chem. Biol. 5 (2009) 15–22.
[37] D. Zheng, N. Ezzeddine, C.-Y.A. Chen, W. Zhu, X. He, A.-B. Shyu, Deadenylation is prerequisite for P-body formation and mRNA decay in mammalian cells, J. Cell Biol. 182 (2008) 89–101.
[38] J.Y. Youn, W.H. Dunham, S.J. Hong, J.D.R. Knight, M. Bashkurov, G.I. Chen, H. Bagci, B. Rathod, G. MacLeod, S.W.M. Eng, S. Angers, Q. Morris, M. Fabian, J.F. Cote, A.C. Gingras, High-density proximity mapping reveals the subcellular organization of mRNA-associated granules and bodies, Mol. Cell 69 (2018) 517–532 e511.
[39] M.A. Reijns, R.D. Alexander, M.P. Spiller, J.D. Beggs, A role for Q/N-rich aggregation-prone regions in P-body localization, J. Cell Sci. 121 (2008) 2463–2472.
[40] C.J. Decker, D. Teixeira, R. Parker, Edc3p and a glutamine/asparagine-rich domain of Lsm4p function in processing body assembly in Saccharomyces cerevisiae, J. Cell Biol. 179 (2007) 437–449.
[41] A. Molliex, J. Temirov, J. Lee, M. Coughlin, A.P. Kanagaraj, H.J. Kim, T. Mittag, J.P. Taylor, Phase separation by low complexity domains promotes stress granule assembly and drives pathological fibrillization, Cell 163 (2015) 123–133.
[42] M. Kato, T.W. Han, S. Xie, K. Shi, X. Du, L.C. Wu, H. Mirzaei, E.J. Goldsmith, J. Longgood, J. Pei, N.V. Grishin, D.E. Frantz, J.W. Schneider, S. Chen, L. Li, M.R. Sawaya, D. Eisenberg, R. Tycko, S.L. McKnight, Cell-free formation of RNA granules: low complexity sequence domains form dynamic fibers within hydrogels, Cell 149 (2012) 753–767.
[43] J.H. Kim, J.D. Richter, RINGO/cdk1 and CPEB mediate poly(A) tail stabilization and translational regulation by ePAB, Genes Dev. 21 (2007) 2571–2579.
[44] W.-J. Lin, A. Duffy, C.-Y. Chen, Localization of AU-rich element-containing mRNA in cytoplasmic granules containing exosome subunits, J. Biol. Chem. 282 (2007) 19958–19968.
[45] A.L. Fink, Natively unfolded proteins, Curr. Opin. Struct. Biol. 15 (2005) 35–41.